https://doi.org/10.5194/acp-2021-936
Preprint. Discussion started: 15 December 2021

Atmospheric Chemistry and Physics Discussions

Volcanic SO_2 Layer Height by TROPOMI/S5P; validation against IASI/MetOp and CALIOP/CALIPSO observations.

Maria-Elissavet Koukouli[1], Konstantinos Michailidis[1], Pascal Hedelt[2], Isabelle A. Taylor[3], Antje Inness[4], Lieven Clarisse[5], Dimitris Balis[1], Dmitry Efremenko[2], Diego Loyola[2], Roy G. Grainger[3] and Christian Retscher[6]

[1] Laboratory of Atmospheric Physics, Aristotle University of Thessaloniki, Greece.
[2] German Aerospace Center (DLR), Remote Sensing Technology Institute, Oberpfaffenhofen, Germany.
[3] COMET, Sub-department of Atmospheric, Oceanic and Planetary Physics, University of Oxford, UK.
[4] European Centre for Medium-Range Weather Forecasts (ECMWF), Reading, UK.
[5] Université Libre de Bruxelles (ULB), Spectroscopy, Quantum Chemistry and Atmospheric Remote Sensing (SQUARES), Brussels, Belgium.
[6] European Space Agency, ESRIN, Frascati, Rome.

Corresponding author: Hedelt, Pascal Andre, Pascal.Hedelt@dlr.de

Abstract. Volcanic eruptions eject large amounts of ash and trace gases such as sulphur dioxide (SO_2) into the atmosphere. A significant difficulty in mitigating the impact of volcanic SO_2 clouds on air traffic safety is that these gas emissions can be rapidly transported over long distances. The use of space-borne instruments enables the global monitoring of volcanic SO_2 emissions in an economical and risk-free manner. Within the European Space Agency (ESA) Sentinel-5p+ Innovation project, the S5P SO_2 Layer Height (S5P+I: SO_2 LH) activities led to the improvements on the retrieval algorithm and generation of the corresponding near-real-time S5P SO_2 LH products. These are currently operationally provided, in near-real-time, by the German Aerospace Center (DLR) in the framework of the Innovative Products for Analyses of Atmospheric Composition, INPULS, project. The main aim of this paper is to present its extensive verification, accomplished within the S5P+I: SO_2 LH project, over major recent volcanic eruptions, against collocated space-born measurements from the IASI/Metop and CALIOP/CALIPSO instruments, as well as assess its impact on the forecasts provided by the Copernicus Atmospheric Monitoring Service, CAMS. The mean difference between S5P and IASI observations for the Raikoke 2019, the Nishinoshima 2020 and the La Soufrière-St Vincent, 2021 eruptive periods is ~0.5±3km, while for the Taal 2020 eruption, a larger difference was found, between 3 and 4±3km. The comparison of the daily mean SO_2 layer heights further demonstrates the capabilities of this near-real-time product, with slopes between 0.8 and 1 and correlations ranging between 0.6 and 0.8. Comparisons between the S5P+I: SO_2 LH and the CALIOP/CALIPSO ash plume height are also satisfactory at -2.5±2km, considering that

https://doi.org/10.5194/acp-2021-936
Preprint. Discussion started: 15 December 2021


Atmospheric Chemistry and Physics Discussions

the injected SO_2 and ash plumes' locations do not always coincide over an eruption. Furthermore, the CAMS assimilation of the S5P+I: SO_2 LH product led to much improved model output against the non-assimilated IASI layer heights, with a mean difference of 1.5±2km compared to the original CAMS analysis, and improved the geographical spread of the Raikoke volcanic plume following the eruptive days.

1 Introduction

Ten years have passed since the ash cloud from the 2010 Icelandic Eyjafjallajokull volcano caused an unprecedented disruption to air traffic across Europe, affecting the flight schedules of approximately 10 million passengers and resulting in nearly 2 billion US dollars in lost airline revenue (Bolić and Sivčev, 2011). This eruption led to increased awareness of the threat of volcanic ash to air traffic in Europe, and numerous advances have taken place since then with regard to research, regulation, and cooperation (Reichardt et al., 2017). Apart from the ash cloud, the volcanic sulphur dioxide (SO_2) plume is also hazardous to aircraft, as it forms the corrosive sulphuric acid and can further deposit sulphates in the engines (Prata, 2009). Since the ash particles will deposit faster than SO_2, after the first post-eruption hours, the two clouds typically separate in elevation, making the reliable detection, dispersal and forecast of both clouds during significant explosive eruptions on a global basis equally important (ICAO, 2012).

The disruption that the Eyjafjallajökull & Grímsvötn 2010 and 2011 eruptions had on airborne traffic has led the International Civil Aviation Organization, ICAO, to change the previous zero tolerance policy on volcanic ash to establishing ash concentration thresholds over Europe. Zehner et al., 2012, have translated these thresholds into specific requirements for improved volcanic ash monitoring and forecasting services. These include the early detection of volcanic emissions and the near real-time, NRT, global monitoring of volcanic plumes, with open access and delivery of data (Brenot et al., 2014; 2021), but also the quantitative retrievals of volcanic ash as well as SO_2 concentration and altitude from satellite instruments, and their validation.

While quantifying the SO_2 load emitted during explosive eruptions provides insight into volcanic processes assists in volcanic hazard mitigation and permits the climatic impact quantification of major eruptions (Carn et al., 2016), the retrieval of the SO_2 plume injection height drives the majority of current scientific advancements in the field. Numerous eruptions have already been used as demonstrational case studies using a variety of space-borne observations and modelling techniques to infer the layer height such as eruptions by Mt Etna, Italy, (Boichu et al., 2015), Nabro, Erithrea, (Clarisse et al., 2014), Jebel at Tair, Yemen (Eckhardt et al., 2008), Eyjafjallajökull and Grimsvötn, Iceland (Carboni et al., 2016), Calbuco, Chile (Pardini et al., 2018), to name but a few.

Within the European Space Agency (ESA) Sentinel-5p+ Innovation SO_2 Layer Height project (S5P+I: SO2LH) activities have led to the generation of a near-real-time SO_2 Layer Height product based on the Sentinel-5P/TROPOMI observations, hereafter referred to as S5P SO_2 LH. In this work, we present the direct validation of the retrieved SO_2 layer heights for four recent

https://doi.org/10.5194/acp-2021-936
Preprint. Discussion started: 15 December 2021


Atmospheric Chemistry and Physics Discussions

major eruptions against independent satellite information as well as its indirect verification via its assimilation into the Copernicus Atmospheric Monitoring Service, CAMS, forecast system.

2 S5P SO_2 Layer Height

The retrieval of the SO_2 layer height based on Sentinel-5P/TROPOMI measurements is performed using the already established "Full-Physics Inverse Learning Machine" algorithm (hereafter referred to as FP_ILM). The FP_ILM algorithm for the retrieval of S5P+I SO_2 LH is based on Hedelt et al., 2019 and is an improvement of the FP_ILM algorithm developed by Efremenko et al., 2017 for the retrieval of the SO_2 LH based on the Global Ozone Monitoring Experiment, GOME-2, instrument data using a Principal Component Regression (PCR) technique. In general, the FP_ILM algorithm creates a mapping between the spectral radiance and atmospheric parameters using machine learning methods. The main advantage of the FP_ILM algorithm over classical direct fitting approaches is that the time-consuming training phase involving complex Radiative Transfer (RT) modelling and Neural Network (NN) training is performed offline; the final trained inversion operator itself is robust and computationally simple and therefore extremely fast and can be applied in near-real-time (NRT) processing environments, as discussed in detail below. The FP_ILM algorithm was originally developed for the retrieval of cloud properties (Loyola et al., 2006) and has also been used for the retrieval of ozone profile shapes (Xu, et al., 2017) as well as the retrieval of surface properties accounting for bidirectional reflectance distribution function (BRDF) effects (Loyola, et al., 2020.) Recently, Fedkin et al., 2020 have applied the FP_ILM algorithm to retrieve the SO_2 LH based on Ozone Monitoring Instrument, OMI/Aura, observations.

The S5P SO_2 LH algorithm was further optimized in the framework of the ESA S5P+I: SO2LH project. The S5P+I project has been initiated to develop novel scientific and operational applications, products and retrieval methods that exploit the potential of the Sentinel-5p mission's capabilities beyond its primary objective and has been kicked-off at the end of June/beginning of July 2019. It will run until the end of 2021 and addresses seven themes related to atmospheric composition and ocean colour. The SO2LH theme is dedicated to the generation of an SO_2 layer height product for Sentinel-5p considering data production timeliness requirements. More details about the project can be found on the ESA S5P+I website (https://eo4society.esa.int/projects/sentinel-5p+innovation/, last access: 14.10.2021) as well as on the dedicated SO_2 LH project website (https://atmos.eoc.dlr.de/so2-lh/, last access: 14.10.2021), where all algorithm and product related documents are publicly available.

2.1 The optimised FP_ILM algorithm description

The FP_ILM SO_2 LH algorithm combines a Principal Component analysis (PCA) and a Neural Network (NN) approach to retrieve the SO_2 LH based on Sentinel-5P/TROPOMI backscattered UV Earthshine measurements in the wavelength range between 311 and 335 nm. The PCA is used to reduce the dimensionality of the high-resolution spectral measurements and to

https://doi.org/10.5194/acp-2021-936
Preprint. Discussion started: 15 December 2021


Atmospheric Chemistry and Physics Discussions

extract the information related to the LH, whereas the NN is used to directly retrieve the LH based on the extracted principal components (PCs) and other input parameters.

In a first step, the FP_ILM algorithm is trained using synthetic spectral UV data generated with the Linearized Discrete Ordinate Radiative Transfer (LIDORT) model including inelastic rotational Raman scattering (RRS) implementation (Spurr et al., 2008). About 500,000 reflectance spectra on a smart parameter grid (Loyola et al., 2016) in the wavelength range 311 - 335 nm have been generated, which are then convolved with the TROPOMI Instrument Spectral Response Function (ISRF). This simulated dataset is split into two datasets: 90% is used for training the PCA and NN and the remaining 10% are set aside and are used as an independent test dataset to determine the accuracy of the FP_ILM training. A PCA is then applied to the training dataset to extract the first N=10 principle components to reduce the dimensionality of the spectral dataset. By thus characterizing the set of simulated measurements with fewer parameters, a simpler, more stable and computationally efficient inversion scheme can be realized.

In the second step, the PCs of each training sample along with the total ozone vertical column density (O_3 VCD), viewing angles, surface pressure and albedo are used as input to train a feedforward artificial NN, with the corresponding SO_2 LH of each training sample as the output layer. The NN consists of two hidden layers consisting of 40 nodes in the first and 10 nodes in the second layer. A hyperbolic tangent layer activation function (tanh) is used and a regularization is applied to prevent the NN from overfitting and to reduce the generalization error. Put together, the trained PCA operator and the trained NN form the FP_ILM inversion operator, which is then applied to real spectral measurements in the operational phase.

In the operational phase, the trained PC operator is applied to TROPOMI spectral measurements which feature enhanced SO_2 levels, such as after a volcanic eruption, to extract the first 10 PCs and thus reduce the spectral dimension. With this information (along with the other measured input parameters) the trained NN inverse function is then applied to retrieve the SO_2 LH. Note that neither the SO_2 SCD nor the SO_2 VCD are input to the NN since they depend on the SO_2 LH both directly and indirectly via the Air Mass Factor calculation and the temperature dependency of the absorption cross-section at the SO_2 layer altitude.

In the operational TROPOMI/S5P ground segment, Level 2 (L2) data is generated within 3 hours after sensing. Once this L2 data is available and a volcanic eruption occurs, the SO_2 LH algorithm is able to retrieve the corresponding layer height within a few milliseconds per ground pixel. Even for a huge volcanic eruption with an SO_2 cloud spanning about 3% of the entire orbit (i.e. about 50,000 pixels), the whole SO_2 LH retrieval is performed within 3 minutes. Note that the largest volcanic eruptions detected by satellites so far (e.g., Raikoke, Kasatochi, Sarychev, Nabro) lead to typically 1-3% of ground pixels to be processed for a limited number of orbits. The FP_ILM algorithm is several orders of magnitude faster than any of the direct fitting approaches for UV layer height retrievals developed so far.

Closed-loop retrievals with the independent test dataset show that the SO_2 LH can be retrieved with an accuracy of less than 2 km for SO_2 VCD > 20DU (see Hedelt et al., 2019; SO_2 LH Algorithm Theoretical Baseline Document, ATBD, Hedelt et al., 2021 and SO_2 LH Validation Report, VR, Koukouli et al., 2021). Note here that in the presence of volcanic ash, which can be initially collocated with the SO_2 cloud in the young volcanic plume, the retrieved SO_2 LH can be underestimated by several

https://doi.org/10.5194/acp-2021-936
Preprint. Discussion started: 15 December 2021


Atmospheric Chemistry and Physics Discussions

kilometres since the FP_ILM inversion operators were trained without taking ash absorption into account (see an extensive discussion in SO_2 LH ATBD, Hedelt et al. 2021).

From the analysis presented in the SO_2 LH VR (Koukouli et al., 2021) it was deduced that the optimal accuracy was achieved when filtering the reported LH values using a QA value (indicating the quality of the retrieval) greater than 0.5, a LH flag (indicating warnings and errors during the retrieval) less than 16 and an associated SO_2 load greater than 20 D.U. For the comparison against the independent datasets, the SO_2 LH were then gridded onto a 0.1x0.1° spatial plane at 6h intervals per eruptive day.

3 Comparative datasets

Two different IASI/Metop SO_2 layer heights (LHs) are used for the validation of the S5P SO_2 LHs: the EUMETSAT ACSAF Brescia v201510 product (Clarisse et al., 2012; 2014; Astoreca et al., 2018), here after IASI ULB/LATMOS, as well as the University of Oxford product (Carboni et al., 2012; 2016), hereafter IASI AOPP. The two IASI approaches vary to such an extent, as is discussed below, that we can assume that they provide two semi-independent datasets available for the validation of the S5P SO_2 LHs. In addition, the CALIOP/CALIPSO space-born lidar observations of the ash plume (Winker et al., 2012; Prata et al., 2017) will be compared to the S5P SO_2 LHs for the case of the Raikoke stratospheric eruption. Furthermore, the S5P SO_2LH product was assimilated into a Copernicus Atmosphere Monitoring Service, CAMS, experiment (Inness et al., 2021), and the assimilated fields were compared to the independent IASI ULB/LATMOS observations, indirectly validating the S5P SO_2 LH v4.0 product.

3.1 IASI ULB/LATMOS SO_2 Layer Height dataset

The IASI/MetOp SO_2 ACSAF column data are fully described in Clarisse et al., 2012, where a algorithm for the sounding of volcanic SO_2 plume above ~5 km altitude was presented and applied to IASI. The algorithm is able to view a wide variety of total column ranges (from 0.5 to 5000 D.U.), exhibits a low theoretical uncertainty (3–5 %) and near real time applicability and was thence demonstrated on the eruptions of Sarychev in Russia, Kasatochi in Alaska, Grimsvötn in Iceland, Puyehue-Cordon Caulle in Chile and Nabro in Eritrea. Furthermore, an expansion of the algorithm to also provide SO_2 LHs for the Nabro eruption using forward trajectories and CALIOP coincident measurements is described in Clarisse et al., 2014. The IASI ULB/LATMOS dataset includes five SO_2 column data at assumed layer heights of 7, 10, 13, 16 and 25 km, as well as a retrieved best estimate for the SO_2 LH. It is important to note that the SO_2 LHs provided by this algorithm are quantized every 0.5km, which renders simple scatter-type comparisons not as straightforward. This dataset is publicly available from https://iasi.aeris-data.fr/

The observations by all Metop IASI instruments were treated as one, gridded onto a 0.1x0.1 grid at 6h intervals or each day. The choice of the temporal field was applied since the S5P and Metop orbits differ on average by 3-4h and this temporal range

https://doi.org/10.5194/acp-2021-936
Preprint. Discussion started: 15 December 2021


Atmospheric Chemistry and Physics Discussions

was found to be the optimal trade-off between resulting in a successful collocative dataset while also ensuring the comparisons view the same parts of the SO_2 plumes. Recall also that IASI, an infrared sounder, also performs observations 12h later, during night-time. For high enough latitudes, the time zones collapse onto another, so in the case of high latitude volcanoes, such as Raikoke, a collocation closer in time can be achieved. For this dataset, the reported SO_2 LHs were restricted to altitudes less than 25km where a successful SO_2 column retrieval was performed.

3.2 IASI AOPP SO_2 Layer Height dataset

The University of Oxford employs an optimal estimation scheme (Carboni et al. 2012; 2016) to estimate the SO_2 column amount, the height of the SO_2 profile and the surface radiating temperature from IASI/MetOp-A, /MetOp-B & /MetOp-C measurements. The Oxford retrieval has two steps. Firstly, a linear retrieval developed by Walker et al. (2011; 2012) is applied. In the retrieval scheme a detection is considered 'positive' if the output of the linear retrieval is greater than a defined positive threshold (0.49 effective DU, following Walker et al. 2012). The detection limits are variable-dependent on the height of the plume and the atmospheric conditions. For a standard atmosphere (with no thermal contrast) the detection limits are estimated to be: 17 DU for a SO_2 plume between 0-2 km, 3 DU between 2-4 km, and 1.3 DU between 4-6 km (Walker et al., 2011). The detection scheme can miss part of an SO_2 plume under certain circumstances, such as low-altitude plumes, conditions of negative thermal contrast (i.e. where the surface is colder than the atmosphere), and where clouds are present above the SO_2 plume, masking the signal from the underlying atmosphere. Secondly, an iterative retrieval is performed for the pixels that provide positive detection results. The scheme iteratively fits the forward model (simulations) with the measurements, through the error covariance matrix, to seek a minimum of a cost function. The forward model is based on RTTOV (Radiative Transfer for TOVS) which is a very fast radiative transfer model for passive visible, infrared and microwave downward-viewing satellite radiometers, spectrometers and interferometers (Saunders et al., 1999). The error covariance matrix used is the 'global error covariance matrix' described by Carboni et al., 2012, defined to represent the effects of atmospheric variability not represented in the forward model (FM), as well as instrument noise. A quality control is usually applied to the dataset; these are values where the minimization routine converges within 10 iterations, the SO_2 amount is positive, the plume pressure is between 0 and 1100 mb and the cost function is less than 10. A comprehensive error budget for every pixel is included in the retrieval. The IASI SO_2 retrieval is not affected by underlying clouds.

The IASI/AOPP dataset was also gridded onto a 0.1x0.1 grid at 6h intervals per eruptive day. An additional filter was applied if the SO_2 LH $\leq$ 25km, the SO_2 LH error $\leq$ SO_2 layer height and the retrieved altitude $\neq$ apriori altitude at 400 mbars, which would indicate that the retrieval reverted back to the a priori for lack of signal in the measurement.

3.3 CALIOP/CALIPSO Volcanic Layer Height dataset

CALIPSO (*Cloud-Aerosol and Lidar Infrared Pathfinder Observations)*, is a joint NASA/CNES (Centre National d' Études Spatiales) satellite and part of the A-Train constellation of satellites. It is designed to study aerosols and clouds and aims to

https://doi.org/10.5194/acp-2021-936
Preprint. Discussion started: 15 December 2021


Atmospheric Chemistry and Physics Discussions

provide profiling information at a global scale for improving our knowledge and understanding of the role of the aerosols in the atmospheric processes. The main instrument, CALIOP (*Cloud-Aerosol Lidar with Orthogonal Polarization)*, is a dual-wavelength (532 and 1064 nm) elastic backscatter lidar with the capability of polarization-sensitive observations at 532 nm (Winker et al., 2010). The high-resolution profiling ability coupled with accurate depolarization measurements make CALIPSO an indispensable tool to monitor specific aerosol species and clouds (Liu et al., 2008). The optical properties retrieval is based on the successful cooperation of three modules whose main mission objective is to produce the CALIPSO Level 2 data. CALIPSO is the first polarization lidar to provide global atmospheric measurements and is able to identify volcanic eruption plumes related to the SO_2 Layer Height identification and retrieval (e.g. Fedkin et al., 2021; Hedelt et al., 2019; Koukouli et al., 2014; Tournigand et al., 2020). The CALIPSO observations close to the volcanic source can be employed in SO_2 LH validation studies, since ash (and/or aerosols) are initially collocated with the SO_2 cloud, before the gas and ash plumes separate. Note that the footprint of CALIOP measurements is only 100m, hence the global coverage is very low and detection of a volcanic ash plume is rare.

CALIPSO data consist of three basic types of information: (a) layer products, (b) profile products and (c) the vertical feature mask (VFM). Layer products provide layer-integrated or layer-averaged properties of detected aerosol and cloud layers. Profile products provide retrieved extinction and backscatter profiles within these layers. Because information on the spatial locations of cloud and aerosol layers is of fundamental importance, the VFM was developed to provide information on cloud and aerosol locations and types. Layer properties include layer top and base altitude, as well as physical properties of the feature such as the Integrated Volume Depolarization Ratio, some of which are described below. Layer top and base altitudes are reported in units of kilometres above mean sea level. Between -0.5 km and ~8.2 km, the vertical resolution of the lidar is 30-meters. From ~8.2 km to ~20.2 km, the vertical resolution of the lidar is 60-meters. Above ~20.2 km, the vertical resolution is 180-meters. The on-board averaging scheme provides the highest resolution in the lower troposphere where the spatial variability of clouds and aerosols is the greatest and coarser resolutions higher in the atmosphere The CALIPSO data products used in this validation study are summarized in Table 1.

Table 1. CALIOP/CALIPSO parameters used in this study.

Parameter	Version	Level	Resolution Due to Averaging	
			Horizontal	Vertical (<8km)
Total_Attenuated_Backscatter_532	v.4.10	1	1/3 km	30 m
Extinction_Coefficient_532	v.3.41, v.4.20	2	5 km	60 m
Aerosol Layer_Top/Base_Altitude	v.3.41, v.4.20	2	5 km	30 m
Feature_Clarification_Flags	v.3.41, v.4.20	2	5 km	60 m

https://doi.org/10.5194/acp-2021-936
Preprint. Discussion started: 15 December 2021


Atmospheric Chemistry and Physics Discussions

The CALIPSO version 4 (V4) product determines the locations of layers within the atmosphere, discriminates aerosols from clouds and categorizes aerosol layers as one of eleven subtypes, seven in the troposphere and four in the stratosphere (Omar et al., 2009; Kim et al., 2018) providing also the optical depth of each detected aerosol layer (Winker et al., 2012). The most fundamental update in V4 is that aerosol layers are now classified as either tropospheric aerosol or of certain stratospheric aerosol feature types. The tropospheric aerosol types include the following sub-types: clean marine, dust, polluted, continental/smoke, clean continental, polluted dust, elevated smoke and dusty marine. Stratospheric aerosol subtypes have been introduced for ash, sulfate/other, smoke and polar stratospheric aerosol. Note that below the tropopause, ash and sulphate plumes are given by the tropospheric aerosol subtypes: volcanic ash is often classified as dust or polluted dust and volcanic sulphate is often classified as elevated smoke. As a result, contiguous aerosol features crossing the tropopause will have aerosol subtypes which switch from tropospheric to stratospheric subtypes, depending on the relationship between the attenuated backscatter centroid altitude of the layer identified by the feature finder and the tropopause altitude. Refer to the Data Quality Summary Document for further details (Vaughan et al., 2020).

3.3.1 CALIOP weighted extinction height

An important indicator for vertical profiles is the weighted extinction height, a parameter that gives in a single number an indication of the altitude of the detected aerosol plume distribution. This parameter is considered ideal for comparisons with aerosol layer height from passive satellite sensors (e.g. GOME-2, IASI, TROPOMI and the future Sentinel missions, since these retrievals are very sensitive to the location of the aerosol mass maximum within the detected layers. For the validation of the TROPOMI SO_2 LH, we used CALIOP level 2 version 4.10 aerosol extinction profiles at 5 km spatial resolution, retrieved from CALIOP observations of attenuated backscatter at 532 nm (Winker et al., 2010). To facilitate quantitative comparison of aerosol altitude, we used a mean extinction height calculated from the CALIOP extinction profile, following Koffi et al. (2012):

$$ALH_{ext} = \frac{\sum_{i=1}^{n} \beta_{ext,i} \cdot Z_i}{\sum_{i=1}^{n} \beta_{ext,i}} \qquad \text{Equation 1}$$

where Z_i is the height from sea level in the i^{th} lidar vertical level i (km), and $\beta_{ext,i}$ is the aerosol extinction coefficient (km^{-1}) at the same level. In the CALIOP level 2 products, aerosol extinction is only retrieved for the layers in which aerosols are detected, depending on the instrument's signal-to-noise ratio (SNR). In the case when aerosols are present over clouds, ALH_{ext} will be situated in the centre of the aerosol layer, with any undetected aerosol layers below the cloud layer not included in the calculations due to attenuation of the signal beyond the cloud layer. According to this validation method, the CALIOP 532nm channel observations are chosen for analysis as the conclusions from the analysis of the results do not change when the 1064 nm channel observations are used instead (Nanda et al., 2020).

https://doi.org/10.5194/acp-2021-936
Preprint. Discussion started: 15 December 2021

Atmospheric Chemistry and Physics Discussions

238 # 4 Results

239 ## 4.1 Comparisons with the IASI/Metop SO_2 Layer Heights

240 ### 4.1.1 Raikoke, 2019

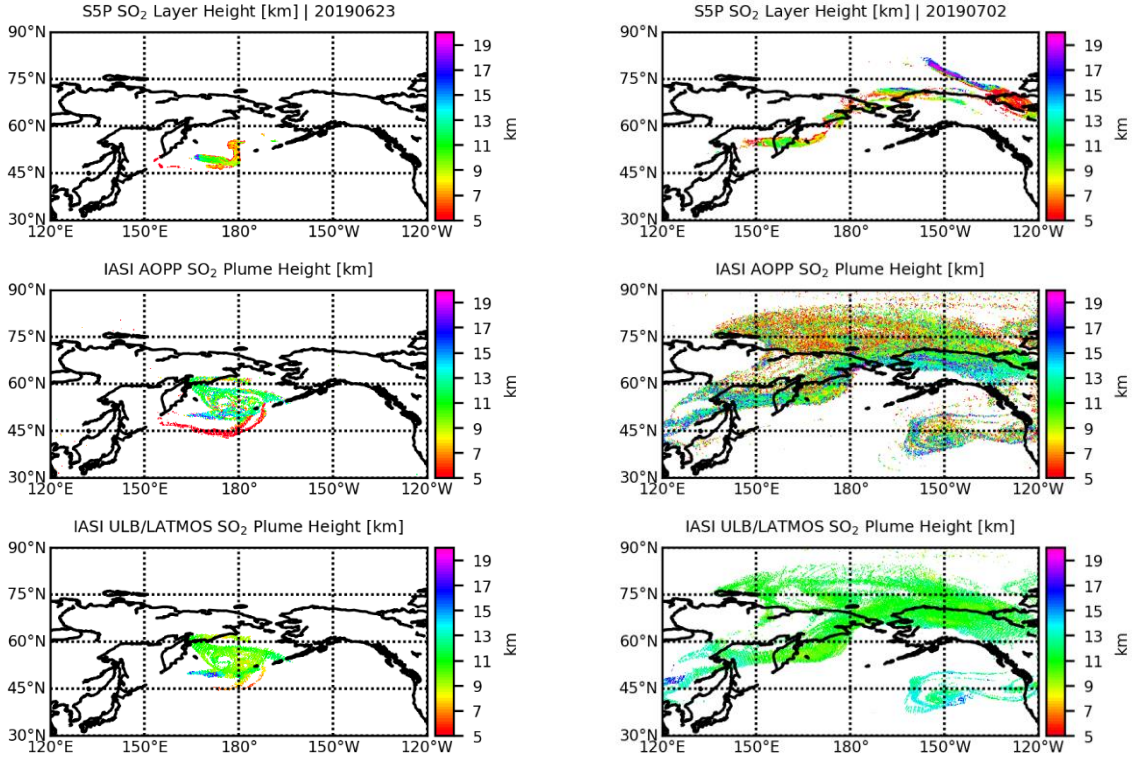

241 **Figure 1.** SO_2 Plume Height for two example days of the Raikoke 2019 eruptive period, the 23rd of June on the left and the 2nd of July on
242 the right. The S5P+I: SO_2 LH at the top, IASI AOPP LH in the middle and IASI ULB/LATMOS LH on the bottom panels, both ascending
243 and descending orbits.

244

245 On June 22nd, 2019, a vast plume of ash and volcanic gases with more than 1000 DU of SO_2 was emitted during the eruption
246 of the Raikoke volcano, Kuril Islands (McKee et al., 2021). This eruption could be detected even two months after the end of
247 eruptive event, which rendered it an important case study for testing different satellite observations retrieval methods; the
248 original FP_ILM methodology applied to TROPOMI observations (Hedelt et al., 2019), a probabilistic enhancement method
249 using the Cross-track Infrared Sounder (CrIS) on the Joint Polar Satellite System (JPSS) series of satellites (Hyman and
250 Pavolonis, 2020), a synergistic analysis of different satellite observations and dispersion modelling (Kloss et al., 2021) and
251 the recent application of the FP_ILM algorithm to OMI/Aura observations (Fedkin et al., 2021.) This eruption was also used

https://doi.org/10.5194/acp-2021-936
Preprint. Discussion started: 15 December 2021

Atmospheric Chemistry and Physics Discussions

in numerical atmospheric modelling in simulating the dispersion of the Raikoke SO_2 cloud in the UK Met Office Numerical Atmospheric-dispersion Modelling Environment (de Leeuw et al., 2021) and the Copernicus Atmosphere Monitoring Service (Inness et al., 2021).

In Figure 1, two example days of the 2019 Raikoke eruption, the 23rd of June (left) and the 2nd of July (right) are shown for the S5P SO_2 LH (upper), the IASI AOPP LH (middle) and the IASI ULB/LATMOS LH (bottom) observations. These demonstrational figures do not represent collocative datasets, but rather show the spatial extent of the plumes reported by each dataset, after filtering and gridding are performed. Due to the restriction in SO_2 load necessary (> 20 D.U.) in the S5P SO_2 LH algorithm, the thinner parts of the plumes are not captured by the S5P observations, however its near-real-time capabilities renders it an excellent tool for early detection in view of aviation safety. The equivalent maps for the SO_2 load are presented in Figure S1, where it is shown that the extensive plumes reported by both IASI products are associated with loads of less than ~20 D.U.

The vertical distribution of the Raikoke SO_2 plume can be examined in the integrated SO_2 mass profiles presented in Figure 2. The reported SO_2 load was integrated every 1km, between 0 and 20km, on the collocated gridded datasets. In these two eruptive days, we note how the SO_2 mass dispersed is placed with respect to the retrieved layer height among the three datasets. Overall, the location of the peak SO_2 mass is within 2km between S5P and IASI, however for the case of the IASI AOPP the amount of ejected SO_2 mass is systematically lower in magnitude, even though it is well placed in height. This is most likely linked to the quality control applied to the IASI AOPP SO_2 results which excludes a number of pixels within the core part of the plume, due to the poor fit between the measured and modelled spectra.

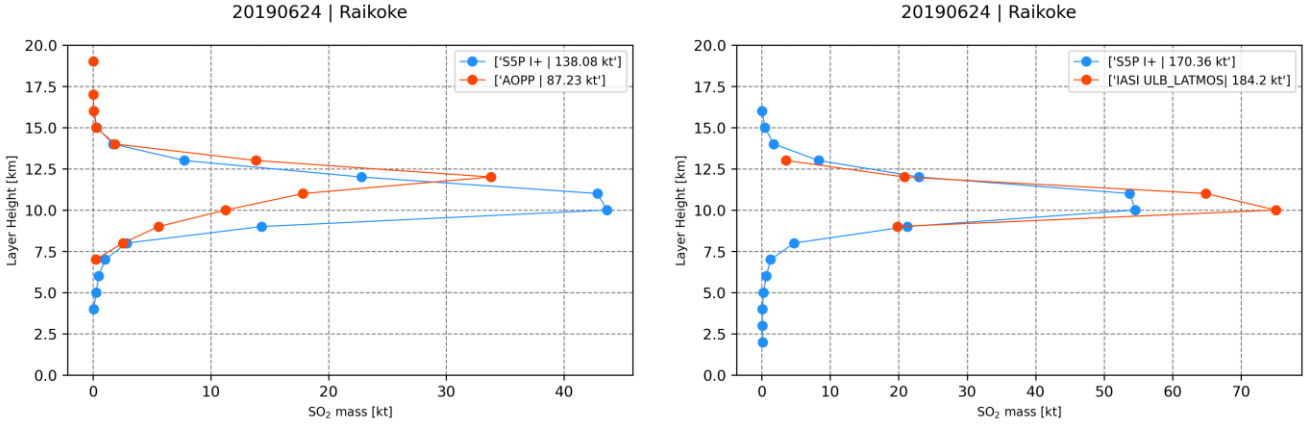

https://doi.org/10.5194/acp-2021-936
Preprint. Discussion started: 15 December 2021

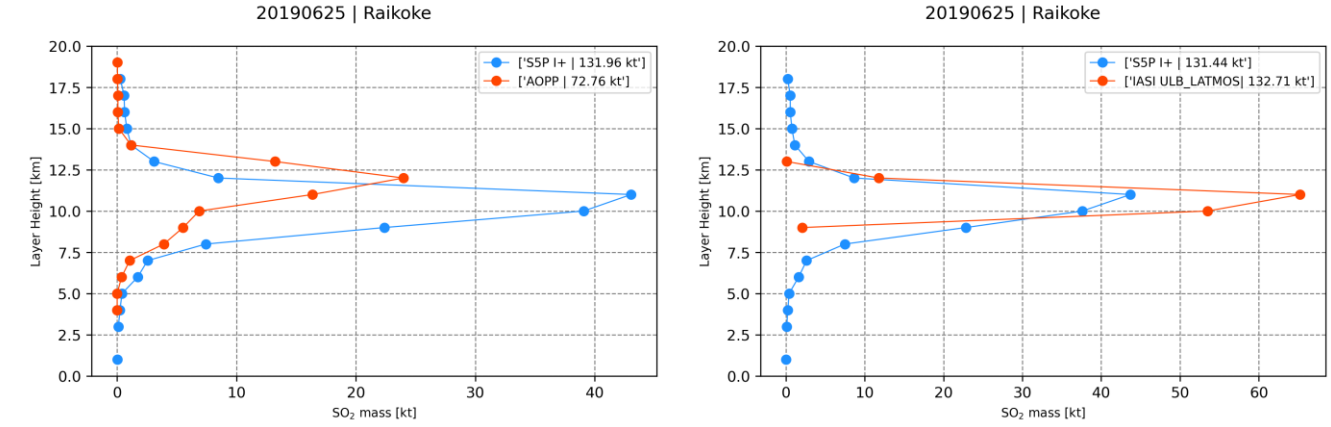

271 **Figure 2.** SO_2 integrated mass (kt) against plume altitude (km) for two example days of the Raikoke 2019 eruptive period, the 24th (upper
272 row) and the 25th of June (lower row) for the S5P+I: SO_2 product in blue and the IASI AOPP in red (left column) and IASI ULB/LATMOS
273 in red (right column). In each set, the respective collocations are shown.

274 Figure 3 shows the comparisons for the entire Raikoke eruptive period between the S5P SO_2 LH and the IASI/AOPP PH (left)
275 and the IASI ULB/LATMOS PH (right) in histogram mode. For both comparisons, the mean S5P SO_2 LH is reported at
276 10±3km, with IASI/AOPP placing the plume at 10±1km and IASI ULB/LATMOS at 11±2.5km, resulting in an excellent mean
277 difference between sensors of ~ ±0.5±3km.
278

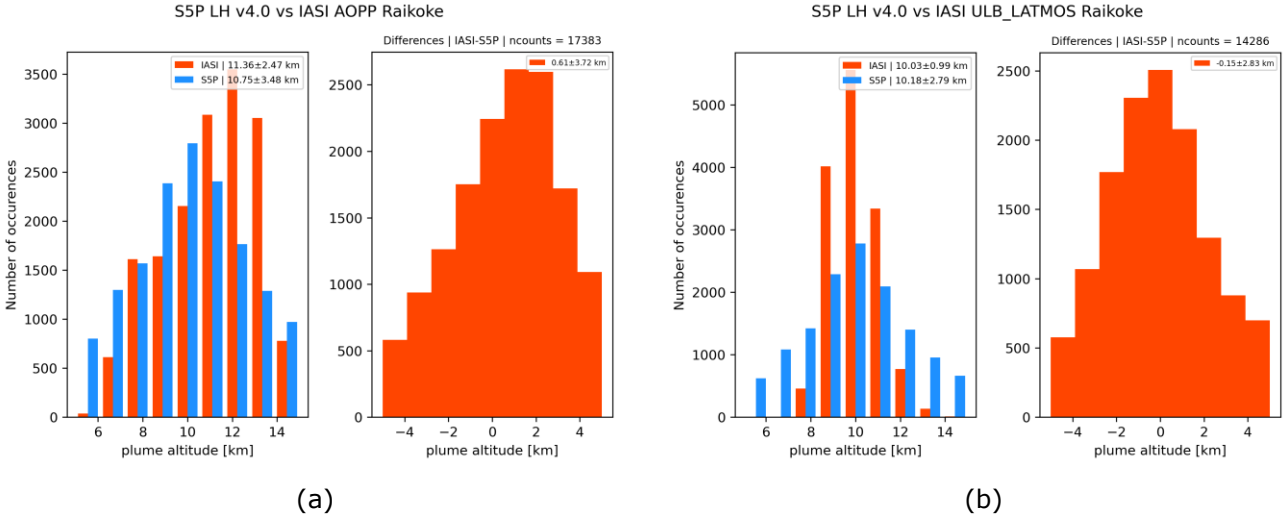

279 **Figure 3.** Comparisons between spatiotemporally collocated plume heights for the Raikoke, 2019, eruptive days. (a), left panel, histogram
280 distribution for the S5P LHs (blue) and the IASI/AOPP LHs (orange) and right panel, their absolute differences. (b) as per (a) for the
281 comparisons to the IASI ULB/LATMOS dataset.

https://doi.org/10.5194/acp-2021-936
Preprint. Discussion started: 15 December 2021


Atmospheric Chemistry and Physics Discussions

4.1.2 Taal, 2020 and La Soufrière, 2021 eruptions

The Taal volcano in Batangas, Philippines erupted on the afternoon of January 12th, 2020, 43 years after its previous eruption in 1977. Stronger explosions began around 3 pm and spewed an ash column exceeding a kilometre high. By 7:30 pm, volcanic activities intensified as continuous eruptions generated a tall 10 to 15 kilometres steam-laden tephra column (Jing et al., 2020). Perttu et al., 2020, analysed infrasound observations to the East of the volcano and estimated a plume height and duration for further ash dispersion modelling, reporting the plume at a mean height of 15km. The High Spectral Resolution Lidar of the Manila Observatory (http://www.observatory.ph/2020/01/17/taal-volcano-2020-eruption-impact-on-air-quality-part-i/, last access 13.10.2021) reported a massive ash cloud ingested and transported above the 12km altitude in the first post eruption hours, a finding further corroborated by the volcanic ash detected by the Advanced Meteorological Imager on board the GEOKOMPSAT-2A platform (Ahn et al., 2021) whose analysis also placed the ash cloud at 12km. The presence of ash hinders the detection of the SO_2 cloud by both UV-visible and infrared sensors and partially explains the larger spread in reported SO_2 layer heights by TROPOMI and IASI shown in Figure S2. A large disagreement on the location of the SO_2 plume is found between datasets in this case, with differences between -3 and -5km between the observations, also attributable to the ~3h difference in sensing time and its importance when studying the first few hours after a volcanic eruption (see maps in Figure S3).

On the morning of April 9th 2021, the La Soufrière volcano on the Caribbean island of Saint Vincent began erupting, spewing ash at least 7.5 km in the air, for the first time since 1979. The volcano continued to erupt over the next several days, with multiple violent explosions. Ash blanketed Saint Vincent and winds carried ash to Barbados, about 120 miles east. The Smithsonian Institute Global Volcanism Program, https://volcano.si.edu/volcano.cfm?vn=360150, last access: 13.10.2021, reported a period of explosive activity and strong pulses of ash emissions at 03:30 on the 10th April, whose resulting ash plumes rose to ~10-16 km altitude throughout the day. On the 12th of April, at 04:15, another large explosion produced an ash plume that rose to ~13 km altitude. The spread of the SO_2 plume sensed by TROPOMI and both IASI algorithms is shown in Figure S4, where the SO_2 plume reached very high altitudes, above 15km, when close in location to the volcano and decreasing in height as it progressed to the East over the sea. For both comparisons in Figure S5, the agreement of the collocative datasets is within 1km, all instruments placing the SO_2 plume at an average height of 14-15km.

4.1.3 Summary of the comparisons with the IASI/Metop observations

The overall statistics for the comparisons of the SO_2 plume altitude for four eruptions between 2019 and 2021 for S5P and the IASI AOPP comparisons are shown in Table 2 while those of the IASI ULB/LATMOS are given in Table 3. The collocations refer each time to those of each of the two sets. Note that for the Nisinoshima, Japan, eruptive period in July & August 2020, collocations are only available for the IASI ULB/LATMOS datasets. Overall, per eruptive period, the mean plume altitudes are similarly placed by both UV-visible and infrared instruments, with a mean difference within 1km, albeit a high standard deviation, between 2.5 and 4km.

https://doi.org/10.5194/acp-2021-936
Preprint. Discussion started: 15 December 2021

Atmospheric Chemistry and Physics Discussions

Table 2. Overall statistics for the comparison between S5P and IASI AOPP for the eruptive periods.

	Mean S5P LH	Mean IASI AOPP LH	Mean Difference	Collocations no.
Raikoke, 2019	10.75±3.48km	11.36±2.47km	0.61±3.72km	17383
Taal, 2020	10.14±3.5km	5.64±1.5km	-4.49±2.82km	47
La Soufriere, 2021	13.82±2.49km	13.47±3.41km	-0.35±3.55km	25

Table 3. Overall statistics for the comparison between S5P and IASI ULB/LATMOS for the eruptive periods.

	Mean S5P LH	Mean IASI ULB/LATMOS LH	Mean Difference	Collocations no.
Raikoke, 2019	10.18±2.79km	10.03±0.99km	-0.15±2.83km	14286
Taal, 2020	12.13±3.95km	9.51±1.78km	-2.62±3.0km	17
Nishinoshima, 2020	7.73±1.97km	8.0±1.04km	0.27±2.79km	11
La Soufriere, 2021	14.94±3.87km	15.7±1.16km	0.76±3.69km	168

The comparisons between S5P and IASI AOPP SO_2 LHs is shown, in Figure 4, left, and IASI ULB/LATMOS on the right, for all eruptive days where the mean plume height reported for each of the 27 days of collocations is shown as a scatter plot. For the IASI AOPP SO_2 LHs, left, the comparison is very promising, with a slope close to 0.9, y-intercept of 1.2km and correlation coefficient of 0.66 for the 27 collocations days for the Raikoke, Taal and La Soufriere eruptions. The outlier point, where S5P reports a high layer height at ~10km while IASI AOPP reports low at ~5km, belongs to the Taal comparison, discussed previously. For ULB/LATMOS comparison, the mean SO_2 LHs, as expected, follow quite closely a straight line, with slope of ~1 and y-intercept of ~0.8km, and a satisfactory correlation coefficient of 0.73. Nearly 20 days belong to the Raikoke eruptive period, and the rest to the Taal, Nishinoshima (only for ULB/LATMOS) and La Soufriere eruptions.

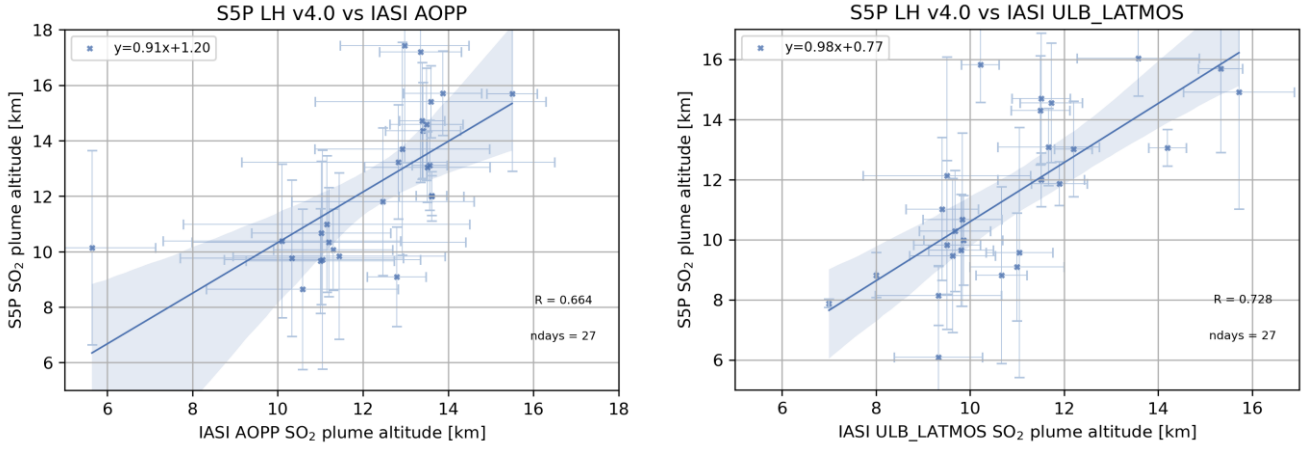

Figure 4. Scatter plot of the mean daily average reported SO_2 LHs by TROPOMI/S5P and IASI/AOPP (left) and IASI ULB/LATMOS (right) for all available collocated eruptive days. The standard error bars represent the standard deviation of the mean.

https://doi.org/10.5194/acp-2021-936
Preprint. Discussion started: 15 December 2021


Atmospheric Chemistry and Physics Discussions

328 **4.2 Comparisons with CALIOP/CALIPSO Volcanic Ash Layer Height**

329 **4.2.1 Raikoke, 2019**

330 Within this study, the availability of overpasses of CALIPSO/CALIOP after the eruption of the Raikoke volcano on the 22nd
331 of June was examined. Volcanic ash and sulphate aerosols are identified in CALIOP profiles based on collocated TROPOMI
332 pixel values. The closest distances between the CALIOP footprint of the CALIPSO overpass and the locations of the
333 TROPOMI centre pixels are selected respectively, to create collocated datasets, usually with the two orbits being within 1h to
334 one another. To illustrate the reliability of the TROPOMI SO_2 LH product, we discuss in detail a selected case of collocated
335 and concurrent TROPOMI – CALIPSO observations close to the detected SO_2 plume from the Raikoke eruption, on the 25rd
336 of June 2019.
337
338 We use the 532 nm Total Attenuated Backscatter (TAB) data version 4.10 from one CALIPSO orbit in order to detect the
339 aerosols and clouds and their heights. The TAB signal strength (Figure 5, top) is color-coded in a manner that the blue
340 background represents molecular and weak aerosol scattering while aerosols typically appear in the shades of red, orange and
341 yellow. The grey scales represent the stronger cloud signals, while the weaker cloud signals, being similar in strength to the
342 strong aerosol signals, also appear in the shades of red, orange and yellow. The TAB is sensitive to both water and ice droplets,
343 as well as numerous types of atmospheric particles. The equivalent VFM image (Figure 5, middle) shows the aerosol type,
344 which is retrieved according to the aerosol classification algorithm for all the detected aerosol layers. The VFM describes the
345 vertical and horizontal distribution of both aerosols and clouds. After detection of the aerosol features, they are then classified
346 into types and subtypes. As shown in Figure 5 (bottom), the plume scene is well captured and according to the V4 algorithm,
347 is classified as volcanic ash/ sulphate (Kim et al., 2018). The volcanic plume of the 25th of June 2019 is marked with a dashed
348 red circle.
349

https://doi.org/10.5194/acp-2021-936
Preprint. Discussion started: 15 December 2021

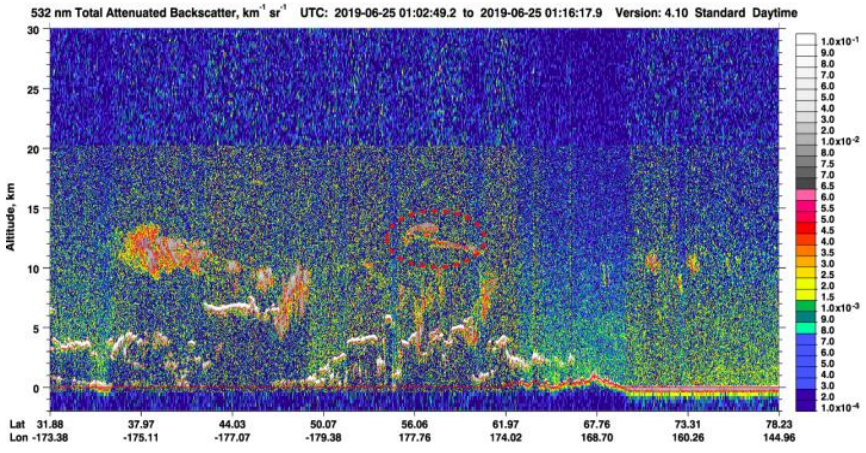

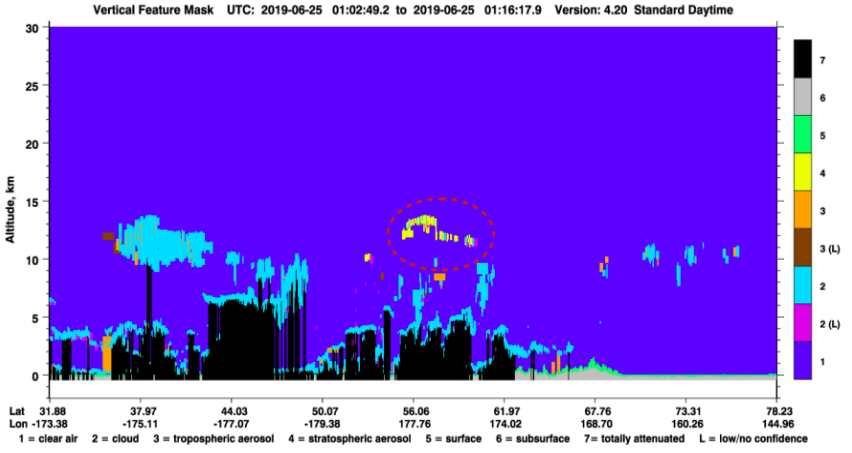

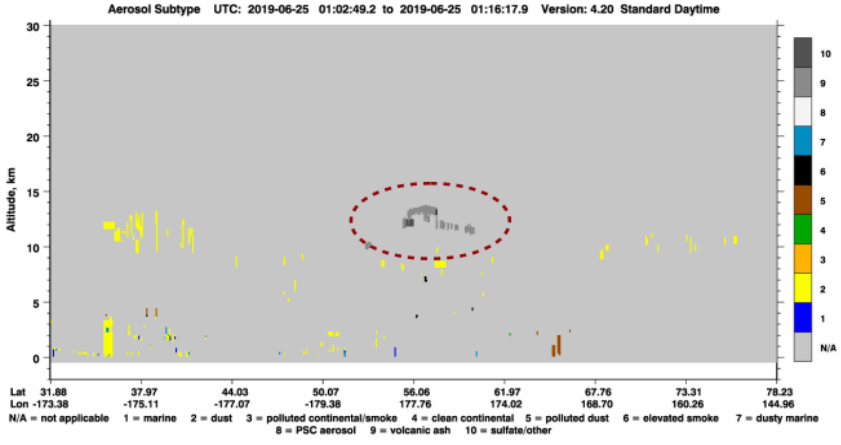

https://doi.org/10.5194/acp-2021-936
Preprint. Discussion started: 15 December 2021

Atmospheric Chemistry and Physics Discussions

Figure 5. (Top) CALIOP total attenuated backscatter profile for the Raikoke eruption on the 25th of June 2019, (middle) Vertical feature mask image showing the location of all layers detected and (bottom) aerosol subtype. The red dashed circles denote the volcanic feature detected from CALIOP. (images from *https://www-calipso.larc.nasa.gov/products/*)

Figure 6 shows the TROPOMI SO_2 layer height pixels retrieved by the FP_ILM algorithm for SO_2 VCDs greater than or equal to 20 DU, QA > 50 and LHflag < 16, overlaid with the calculated CALIPSO weighted extinction ALH pixel values (coloured circles) which are color-coded according to the range of height values (in km). The CALIOP overpass time of this area is between 01:00 and 01:15 UTC, and the TROPOMI overpass time is between 01:25 and 01:30 UTC, a time difference of mere minutes. The TROPOMI plume shows several layers with SO_2 layer heights ranging from 5-6 km up to 14 km for this day. In the area of the plume observed by both TROPOMI and CALIOP (54 – 58°N & 176 – 178°E), the CALIOP vertical feature mask and aerosol subtype mask identify some volcanic ash at approximately 13 km altitude, and meteorological clouds mixed with tropospheric aerosols (dust, polluted dust and elevated smoke) at lower altitudes. The clouds below the ash plume are shown in blue in Figure 5, middle panel.

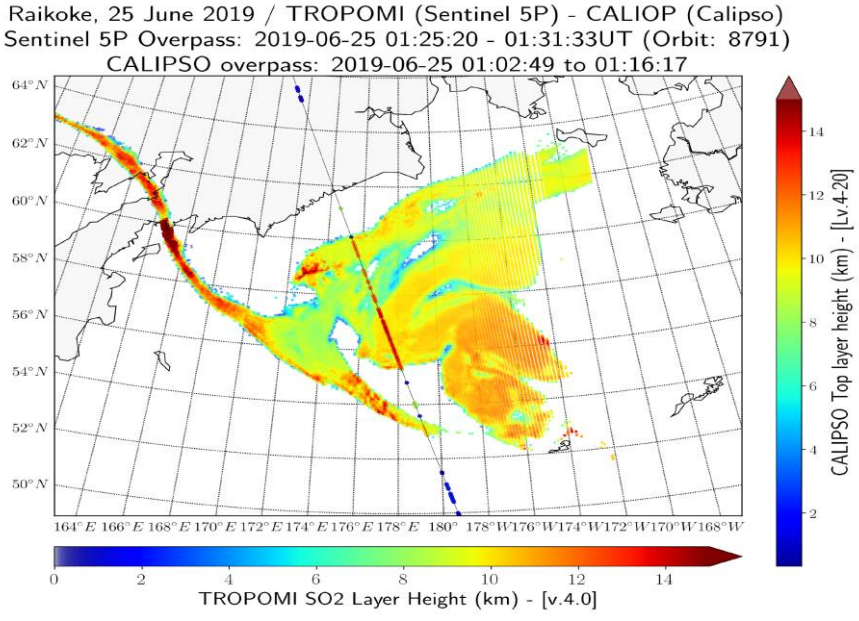

Figure 6. TROPOMI SO_2 layer height for the Raikoke volcanic eruption, measured on the 25th of June 2019. Only pixels with SO_2 VCDs greater than or equal to 20 DU are shown. The black line indicates the CALIPSO ground track and the coloured circles along the line indicate weighted extinction height product values (in km), for the results shown in Figure 5.

https://doi.org/10.5194/acp-2021-936
Preprint. Discussion started: 15 December 2021

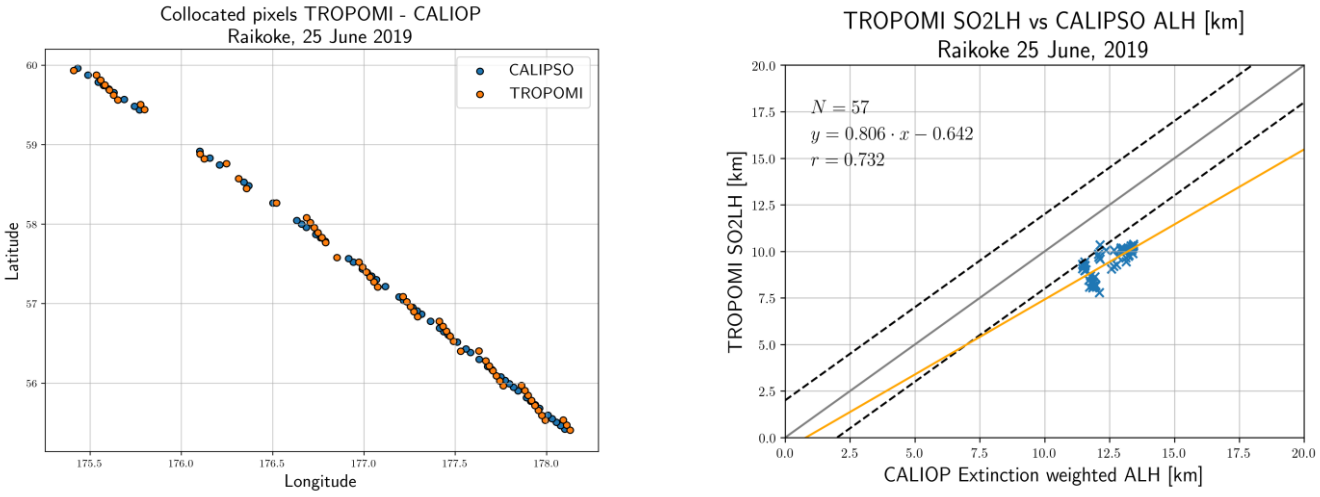

Figure 7. Left. The latitude/longitudes of the collocated pixels. Right. Comparison between TROPOMI SO_2 LH and CALIPSO weighted extinction height for the 25th of June 2019. The orange line is the regression line of the TROPOMI-CALIPSO observations; the grey line is the 1:1 line.

The spatiotemporal collocation between TROPOMI and CALIOP on that day is near perfect (Figure 7, left) and the spatial agreement between SO_2 LH and CALIOP weighted extinction altitude is satisfactory, confirming the presence of volcanic plumes. Both instruments yield high altitude values, however TROPOMI retrieves higher altitudes especially for the western part of the plume. A comparison scatterplot of collocated ash-flagged pixels is shown in Figure 7, right. The pixel-by-pixel scatter of the 57 common points shows a high correlation of 0.73, even though the SO_2 plume is placed approximately 2km lower that the ash plume.

Overall, seven TROPOMI (at 22/6 02:20; 23/6 00:20; 24/6 00:00; 25/6 01:30; 28/6 02:00; 29/6 02:00 and 30/6 01:30) and CALIPSO collocated overpasses (at 22/6 02:30; 23/6 01:30;24/6 00:30; 25/6 01:00; 28/6 03:00; 29/6 03:35 and 30/6 02:40) were identified. A statistical analysis has been performed using all resulting 241 collocated pixels for the 22nd, 23rd, 24th, 25th, 28th, 29th and 30th of June 2019. Figure 8 shows the distribution of TROPOMI SO_2 LH and CALIOP calculated weighted height differences for all days of collocation, as a scatter plot on the left and on a histogram representation on the right. The agreement is quite satisfactory with mean and median residual values around ~-2.4km and ~-3km respectively, and standard deviation of ~1.7km.

https://doi.org/10.5194/acp-2021-936
Preprint. Discussion started: 15 December 2021

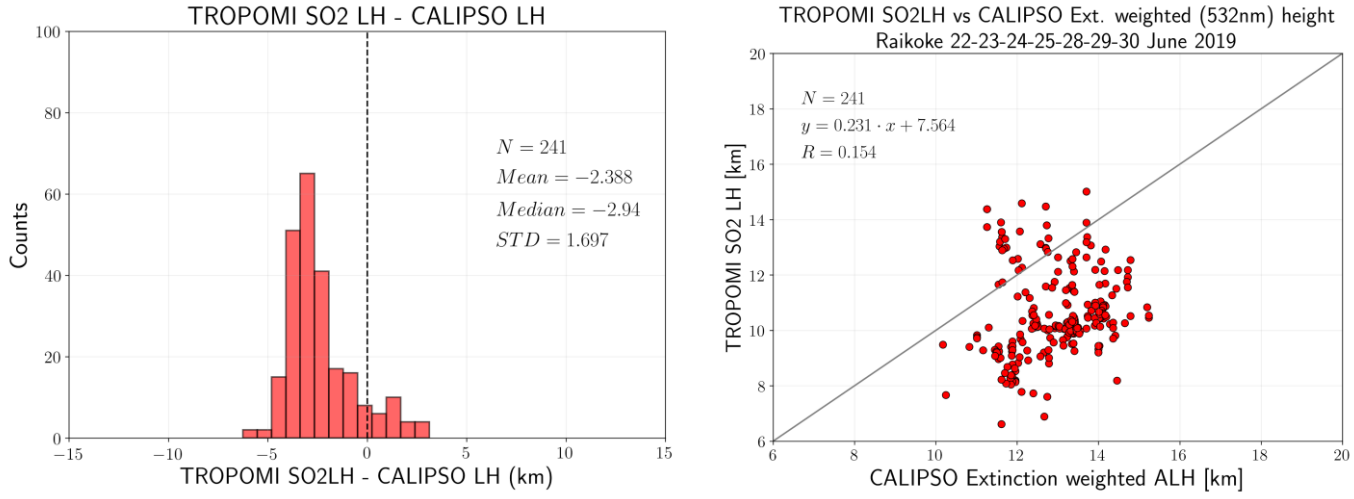

Figure 8. (Left) Scatter plot of the TROPOMI SO_2 LH and CALIPSO weighted height for all collocated pixels on the 22nd, 23rd, 24th, 25th, 28th, 29th and 30th of June 2019, for the Raikoke eruption. (Right) Histogram distribution of the absolute differences between TROPOMI SO_2 LH and the corresponding CALIPSO weighted extinction height measurements, calculated for the 241 collocated points.

4.2.2 Sinabung, 2018, Nishinoshima, 2020 and La Soufrière, 2021 eruptions

On the 19th of February 2018, at 08:53 L.T., the Indonesian stratovolcano Mount Sinabung on Sumatra (2460 m summit elevation) erupted jetting a large ash plume that quickly rose to a heights of approximately 15 to 17km.. Although the eruption was spatiotemporally small an excellent overpass was found against the CALIPSO instrument (Figure S6, left). The CALIOP track crossed the main part of the volcanic cloud, across the north-to-south axis.Its overpass time is between 07:08 and 07:22 UTC, a mere 45 min after the the TROPOMI overpass time, between 06:24 and 06:26 UTC. The CALIPSO observations showed both the ash cloud, as a layer around 5 km, as well as two vertical ash clouds extending from the volcano up to ~10 km altitude. As shown in **Figure 9**, where the S5P SO_2 LH retrievals are shown in the red dots, the presence of clouds appear along the CALIPSO path indicated by the stronger attenuated backscatter than the aerosol layer.

https://doi.org/10.5194/acp-2021-936
Preprint. Discussion started: 15 December 2021

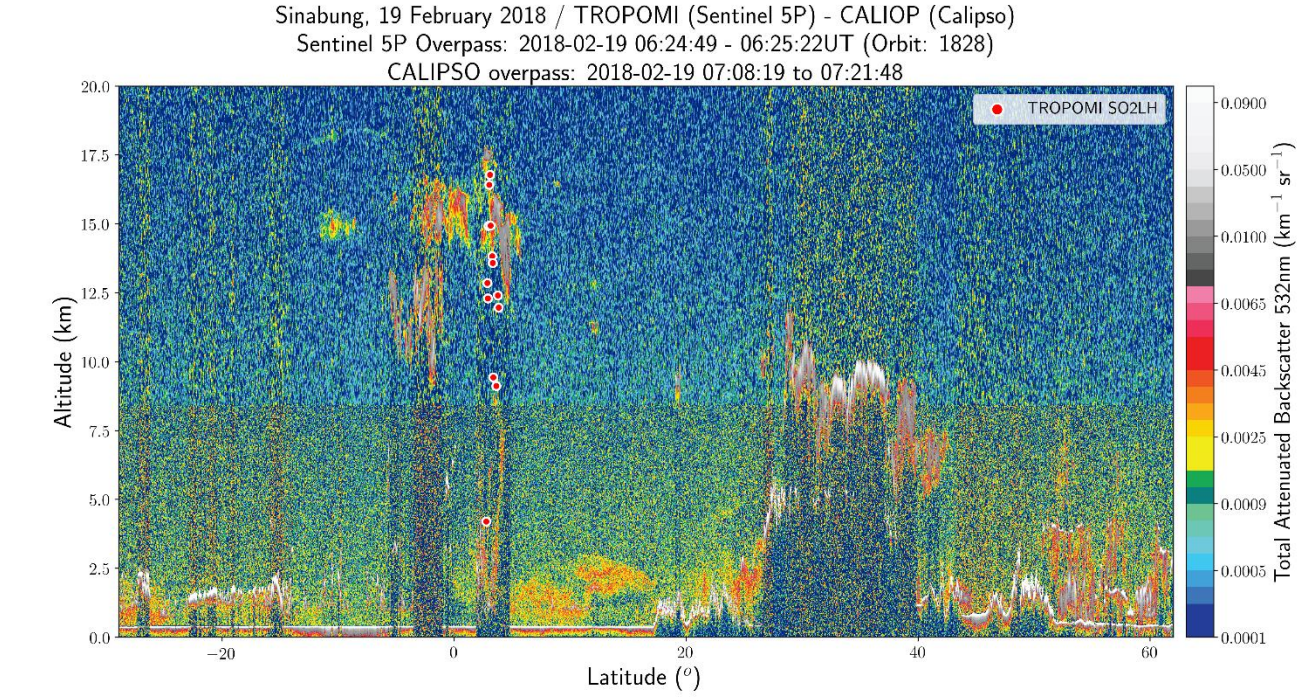

395 **Figure 9.** Sinabung, 19th of February 2018, 07:15 UTC. The colours show the CALIOP/CALIPSO total attenuated backscatter
396 at 532nm and the white-red dots show the TROPOMI SO_2 LH.

397 This case of mixing between ash and clouds over a volcanic eruption renders the retrieval of the ash plume altitude by the lidar
398 algorithm very difficult, since it cannot separate clouds from aerosols, especially when the aerosol amount is low. The
399 CALIPSO feature mask (not shown here) hardly identifies any of the Sinabung backscatter signals as aerosol. The main plume,
400 at ~15km is flagged a cloud feature, while below this feature everything is masked as "totally attenuated", which is not expected
401 to be the case. Most probably liquid water or ice particles are contaminating the volcanic ash signal, as already discussed in
402 Hedelt et al., 2019. Even though the maximum TROPOMI SO_2 LH agrees with the maximum backscatter height between 2-
403 3° latitude, a large spread of TROPOMI SO_2 LHs are also reported. As discussed also in the work of de Laat et al., 2020, the
404 presence of either a nearly-transparent or a bright cloud may result in the TROPOMI algorithm reporting heights far lower
405 than both the ash and the cloud plumes. For the cases of Nishinoshima 2020 and La Soufrière 2021 eruptions, both provided a
406 satisfactory collocation to the CALIOP orbital path without the difficulties found in the case of Sinabung, 2018, enabling a
407 meaningful comparison to be made. For Nishinoshima, spatial collocations for the 1st of August 2020 are shown in Figure S7
408 (left), while the scatterplot of height values is shown in the right. The geographical collocations between TROPOMI and
409 CALIOP are not optimal, however the agreement between SO_2 LH and CALIOP weighted extinction altitude is satisfactory,
410 and tends to confirm the presence of volcanic plumes. The CALIPSO observations confirm the presence of volcanic clouds

https://doi.org/10.5194/acp-2021-936
Preprint. Discussion started: 15 December 2021

Atmospheric Chemistry and Physics Discussions

around 5 km, while S5P reports slightly higher loads, at ~7.5km. For the case of La Soufrière, spatial collocations for the 11st of April 2021 are shown in Figure S8 (left), where the scatterplot of collocations is shown in the right column and the scatter plots in the right column. In this case, both CALIPSO and TROPOMI collocated pixels confirms the presence of a volcanic cloud up to and around ~20km.

4.2.3 Summary of the comparisons with the CALIPSO/CALIOP observations

The combination of CALIOP and TROPOMI data measurements has permitted the identification of volcanic aerosol layers produced by three individual volcanic eruptions. A summary plot of the comparisons between S5P SO2 and CALIPSO ash LHs is presented as a scatter plot in Figure 10, showing the mean ash and SO2 plume height reported for each of the 9 days of collocations. The comparison is very promising, with a slope close to 0.95, y-intercept of ~1 km and correlation coefficient of 0.86 for the 9 collocations days for the Raikoke, Nishinoshima and La Soufrière eruptions. The majority of cases, 7 days, belong nearly to the Raikoke eruptive period, and the remainder 2 days to Nishinoshima and La Soufrière eruptions, respectively. From Table 4 it is worth noting that the standard deviation of the mean heights reported by both instruments are low, typically much less than 1km. This can most likely be attributed to the tight spatiotemporal collocation criteria that were possible for these comparisons.

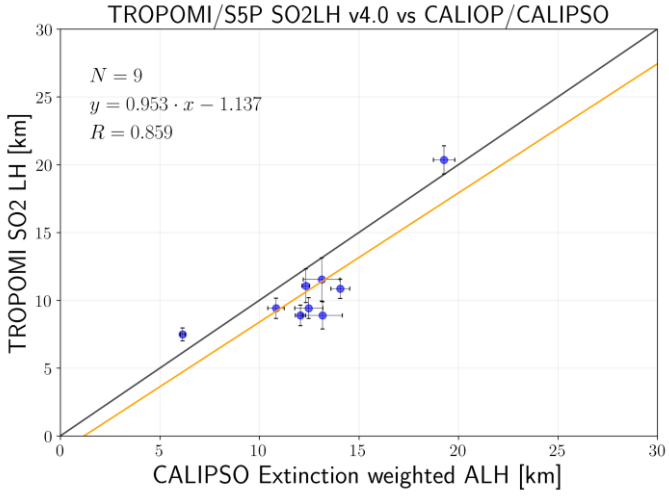

Figure 10. Scatter plot of the mean daily average reported SO_2 LHs by TROPOMI/S5P and CALIOP/CALIPSO for the seven days of the Raikoke eruption and one each for Nishinoshima and La Soufrière eruptions studied.

Table 4. Statistics for the comparison between S5P and CALIPSO for the eruptive days studied.

Eruptive day	Mean CALIPSO LH [km]	Mean S5P Height [km]	Mean Difference [km]	Collocations.

https://doi.org/10.5194/acp-2021-936
Preprint. Discussion started: 15 December 2021


Atmospheric Chemistry and Physics Discussions

22 June 2019	10.84±0.4	9.40±0.75	-1.43±0.56	8
23 June 2019	12.06±0.28	8.88±0.76	-3.17+0.98	13
24 June 2019	12.33±0.2	11.07±1.24	-1.26±1.40	22
25 June 2019	12.47±0.1	9.41±0.76	-3.05±0.54	57
28 June 2019	13.12±0.92	11.53±1.6	-1.59±2.13	87
29 June 2019	14.06±0.47	10.84±0.7	-3.21±0.99	46
30 June 2019	13.16±1	8.88±1	-4.28±0.56	8
01 August 2020	6.14±0.12	7.48±0.48	1.34±0.46	8
11 April 2021	19.28±0.54	20.35±1.04	1.06±1.44	12

Generally, we note that features identified as volcanic ash by the CALIOP aerosol subtype mask are captured by the TROPOMI algorithm, but the surrounding clouds often affect the retrieval. The comparison of the TROPOMI SO_2 LH product within this project shows promising capability in detecting plumes of volcanic origin, with some limitations related to existing or subsequent creation of clouds. Furthermore, although ash and SO_2 plumes are often collocated especially at the first hours after eruptions, this is not always the case, making direct comparisons challenging.

4.3 Application of the S5P SO2 LH in NRT data assimilation modelling

The Copernicus Atmosphere Monitoring Service (CAMS), operated by the European Centre for Medium-Range Weather Forecasts (ECMWF) on behalf of the European Commission, provides daily SO_2 analyses and 5-day forecasts of volcanic SO_2 in NRT by assimilating total column SO_2 retrievals from TROPOMI and GOME-2 (Inness et al., 2021). As the operational NRT TROPOMI and GOME-2 retrievals do not provide any information about the height of the volcanic plumes, the SO_2 increments are placed in the mid-troposphere, around 550 hPa (~5 km) in the current operational CAMS configuration.

https://doi.org/10.5194/acp-2021-936
Preprint. Discussion started: 15 December 2021

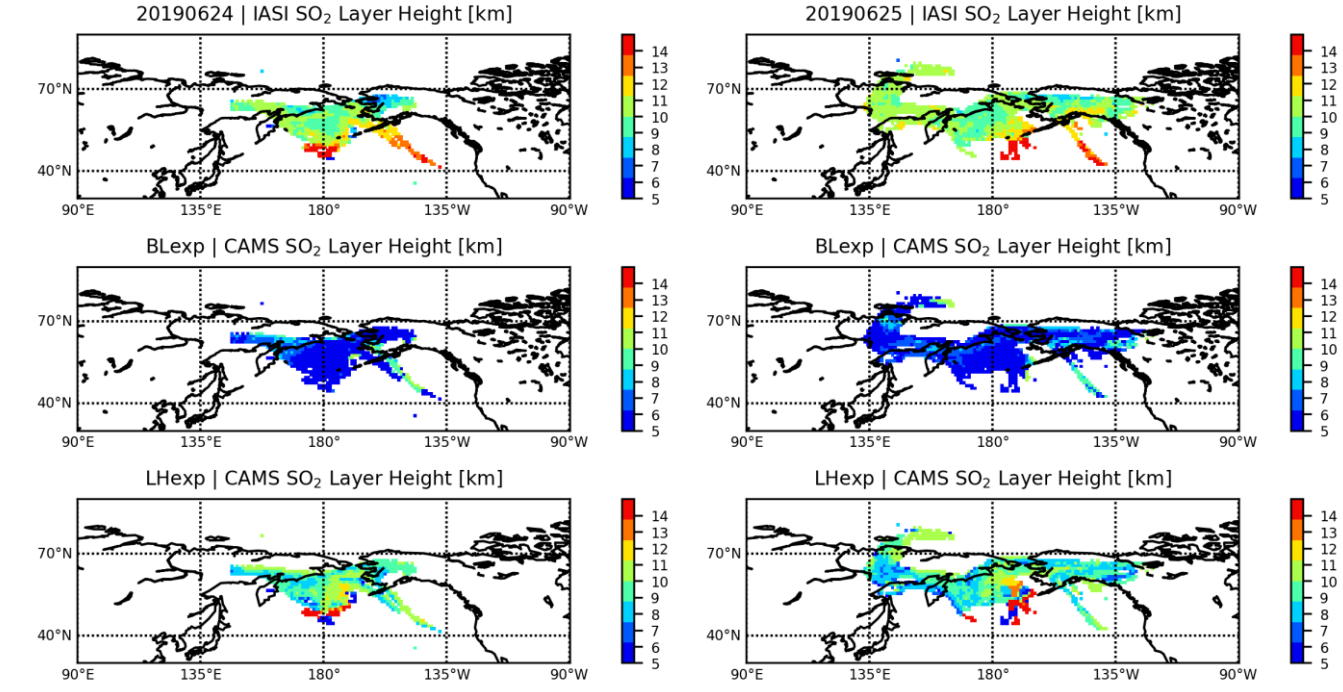

441 **Figure 11.** Raikoke eruptive day of the 24th (left) and 25th (right) of June 2019. Top. The IASI ULB/LATMOS SO_2 layer height in km.
442 Middle. The CAMS BLexp SO_2 layer height. Bottom. The CAMS LHexp SO_2 layer height.

443 In the recent paper by Inness et al., 2021, the procedure used to assimilate near-real time TROPOMI/S5P and GOME2/Metop
444 SO_2 loads in the operational CAMS NRT data assimilation system was presented, alongside the simultaneous ingestion of the
445 S5P SO2LH discussed in this work. The assimilation of the S5P SO_2LH data was based on a previous version of the dataset,
446 v3.1, and not the final one, v4.0, presented in this work. The assimilation was tested for the 2019 Raikoke eruption and was
447 contrasted to the operational CAMS forecasts obtained when assimilating only the TROPOMI SO_2 load. Two example days
448 are shown in this paper. In Figure 11, upper, the IASI ULB/LATMOS SO_2 layer height, gridded onto the CAMS 1x1° spatial
449 resolution and 3h temporal resolution, is shown for the 24th (left column) and the 25th (right column) of June 2019, 5 days after
450 the initial Raikoke eruption. In the middle panel, the operational CAMS SO_2 layer height (called BLexp) is presented which is
451 deduced from placing the SO_2 increment in the mid-troposphere, around 550 hPa, clearly in the wrong altitude for the Raikoke
452 eruption which injected a huge amount of SO_2 above the tropopause, well into the stratosphere. In Figure 11, lower panel, it
453 can be seen that a vast improvement to the CAMS forecast is achieved for both days when the S5P SO_2 LH data are used
454 (called LHexp) as the structure of the Raikoke SO_2 plume is much improved and compares well with the independent IASI
455 SO_2 layer heights shown in the upper panel. For the entire eruptive period of Raikoke between June 22nd and June 29th, the
456 CAMS forecast which assimilates the S5P SO_2 LH data improves the bias in the forecast height between CAMS and IASI to
457 ~ -1.5±2.5km, compared to a mean bias of ~ -5±2km for the operational system. We can hence conclude that by assimilating
458 the S5P SO_2LH data, the vertical location of the Raikoke SO_2 plume in the CAMS system is improved, leading to better

https://doi.org/10.5194/acp-2021-936
Preprint. Discussion started: 15 December 2021


Atmospheric Chemistry and Physics Discussions

459 subsequent forecasts (Inness et al., 2021) and making the S5P SO_2 LH product suitable for NRT assimilation and forecasts of
460 a possible strong future volcanic eruption.

461 5 Conclusions

462 The European Space Agency Sentinel-5p+ Innovation TROPOMI/S5P SO_2 layer height product has been verified against
463 IASI/Metop SO_2 layer heights for the eruptive periods of the Raikoke volcano, 22 June to 30 July 2019, the Taal volcano, 13
464 January 2020, the Nishinoshima eruptive period during July & August 2020 and the La Soufrière eruptive days of April 10th
465 to 11th, 2021. Two different algorithms that provide plume altitude from the IASI instruments were examined, the official
466 EUMETSAT ACSAF algorithm, ULB/LATMOS, and the University of Oxford, AOPP, algorithm. Furthermore, collocations
467 against ash layer height observations by the space-born CALIOP/CALIPSO lidar system were identified and assessed.
468 The main findings in the comparisons of the SO_2 volcanic plumes, described in detail above, are:

469 ▪ For the Raikoke eruptive days: the difference between S5P and IASI/AOPP SO_2 LH datasets is 0.61±3.72km, with
470 IASI/AOPP SO_2 LH reporting a mean height of ~11.5±2.5km and S5P reporting ~10.5±3.5km, in excellent agreement.
471 Between S5P and IASI ULB/LATMOS SO_2 LHs a similar mean difference of ~0±3km is found with both sensors
472 reporting on average LHs at ~10km.
473 ▪ For the Taal eruptive day: the SO_2 LHs reported differ substantially with IASI/AOPP reporting heights ~5.5±1.5km while
474 S5P reports higher columns, at ~10±3.5km. IASI ULB/LATMOS also reports lower heights, at 9.5±2km while and S5P
475 places the plume at ~12±4km with a mean difference of~2.5±3km.
476 ▪ For the Nishinoshima eruptive days: both sensors place the plume at the same altitude, with IASI ULB/LATMOS at
477 ~8±1km and S5P ~8±2km and mean difference of~0±3km.
478 ▪ For the La Soufrière eruptive days: both sensors report high plume altitudes, at ~15km, with both IASI/AOPP and
479 ULB/LATMOS standard deviation at ~1km and the S5P standard deviation at ~4km, and overall mean difference of
480 ~1±3.5km.
481 ▪ Scatter plot comparisons of the daily mean volcanic SO_2 plumes reveal common SO_2 LHs patterns for the two sensors,
482 with substantial correlations ~0.66 (0.72), slope ~0.9 (0.98), y-intercept of 1.2km (0.8km) for the IASI/AOPP and the
483 IASI ULB/LATMOS respectively. The standard deviation of the mean is relatively high, on average ~3km, however the
484 mean heights are well within the 2km accuracy requirement on the S5P SO_2 layer height product.

485 With respect to the comparisons between the S5P SO_2 LH and the CALIOP/CALIPSO volcanic ash layer height, we report
486 that:

487 ▪ 241 excellently spatiotemporally collocated points between CALIOP and TROPOMI were identified for seven Raikoke
488 eruptive days. CALIOP reported a range of mean heights between ~11 and 14km, while TROPOMI had a far narrower
489 range between ~9 and 11.5km. Overall, the mean difference in heights was found to be -2.4±1.7 km (-3.0km median) for
490 the seven eruptive Raikoke days.

https://doi.org/10.5194/acp-2021-936
Preprint. Discussion started: 15 December 2021

Atmospheric Chemistry and Physics Discussions

- The comparisons for the Nishinoshima and La Soufrière eruptions showed good agreement with plumes reported (low) at ~7.km (~19.5km) respectively for the two eruptions, and a height difference between S5P and CALIPSO being within ~1.0km.
- The mean daily height comparative plot of the comparisons between S5P SO_2 LHs and CALIOP/CALIPSO weighted ALH, as expected, follow quite closely a straight line, with slope of 0.95 and y-intercept of ~1.0km and excellent correlation coefficient at 0.86.

Finally, the CAMS assimilation of the NRT S5P SO_2 LH led to much improved model fields against the non-assimilated IASI plume heights for the Raikoke eruptive period, with a mean difference of 1.5±2km against the independent IASI/Metop observations, and improved the geographical spread of the Raikoke volcanic plume following the main eruptive day.

Data availability. The near-real-time S5P SO_2 LH products are operationally generated by DLR in the framework of the Innovative Products for Analyses of Atmospheric Composition, INPULS, project, and are available upon request from Pascal Hedelt (Pascal.Hedelt@dlr.de). The IASI/MetOp ULB/LATMOS open source SO_2 layer height dataset is publicly available from https://iasi.aeris-data.fr/so2_iasi_a_arch/ (last access: 20.07.2021). The IASI/MetOp AOPP SO_2 products are available on request from Isabelle Taylor (isabelle.taylor@physics.ox.ac.uk). The CALIPSO data were obtained from the online archive of the NASA Langley Research Center Atmospheric Science Data Center (ASDC, https://asdc.larc.nasa.gov/project/CALIPSO). The Copernicus Atmosphere Monitoring Service is operated by the European Centre for Medium-Range Weather Forecasts on behalf of the European Commission as part of the Copernicus program (http://copernicus.eu) and CAMS data are freely available from atmosphere.copernicus.eu/data. The SO_2 analysis experiments used in this paper are available from https://apps.ecmwf.int/research-experiments/expver/ with the DOIs: 10.21957/cygt-xf49 (BLexp), 10.21957/qfam-7474 (LHexp).

Acknowledgments This work is performed in the framework of ESA's Sentinel-5p+ Innovation: SO_2 Layer Height project (S5P+I: SO_2 LH), https://eo4society.esa.int/projects/sentinel-5p-innovation-so2-layer-height-project/. The comparative results presented in this work have been produced using the Aristotle University of Thessaloniki High Performance Computing Infrastructure and Resources. M.E.K. would like to acknowledge the support provided by the IT Center of the Aristotle University of Thessaloniki throughout the progress of this research work, as well as the Atmospheric Toolbox®. I.A.T. and R.G.G. would like to acknowledge EUMETSAT for providing the IASI spectra and ECMWF and CEDA for the meteorological profiles used in the IASI retrievals. I.A.T. and R.G.G. further acknowledge support from the NERC Centre for Observation and Modelling of Earthquakes, Volcanoes, and Tectonics (COMET). We thank the DLR Innovative Products for Analyses of Atmospheric Composition, INPULS, project, for continuously providing the S5P SO_2 LH products in near-real-time.

https://doi.org/10.5194/acp-2021-936
Preprint. Discussion started: 15 December 2021


Atmospheric Chemistry and Physics Discussions

522 **References**

523 Ahn S, Jee J-B, Lee K-T, Oh H-J. Enhanced Accuracy of Airborne Volcanic Ash Detection Using the GEOKOMPSAT-2A
524 Satellite. *Sensors*. 2021; 21(4):1359. https://doi.org/10.3390/s21041359.
525 Astoreca R., D. Hurtmans, L. Clarisse, P. Coheur, M. George, J. Hadji-Lazaro and C. Clerbaux, ACSAF Product User Manual
526 for the Near real-time IASI Brescia SO_2 product, SAF/AC/ULB/PUM/002, v1.2, 2018.
527 Balis, D., M. E. Koukouli, Siomos, N., et al., Validation of ash optical depth and layer height retrieved from passive satellite
528 sensors using EARLINET and airborne lidar data: The case of the Eyjafjallajökull eruption, Atmospheric Chemistry and
529 Physics, http://dx.doi.org/10.5194/acp-16-5705-2016, 2016.
530 Boichu, M., Clarisse, L., Péré, J.-C., Herbin, H., Goloub, P., Thieuleux, F., Ducos, F., Clerbaux, C., and Tanré, D.: Temporal
531 variations of flux and altitude of sulfur dioxide emissions during volcanic eruptions: implications for long-range dispersal
532 of volcanic clouds, Atmos. Chem. Phys., 15, 8381–8400, https://doi.org/10.5194/acp-15-8381-2015, 2015.
533 Bolić T, Sivčev Ź. Eruption of Eyjafjallajökull in Iceland: Experience of European Air Traffic Management. Transportation
534 Research Record. 2011;2214(1):136-143. doi:10.3141/2214-17
535 Brenot, H., Theys, N., Clarisse, L., van Geffen, J., van Gent, J., Van Roozendael, M., van der A, R., Hurtmans, D., Coheur,
536 P.-F., Clerbaux, C., Valks, P., Hedelt, P., Prata, F., Rasson, O., Sievers, K., and Zehner, C.: Support to Aviation Control
537 Service (SACS): an online service for near-real-time satellite monitoring of volcanic plumes, Nat. Hazards Earth Syst. Sci.,
538 14, 1099–1123, https://doi.org/10.5194/nhess-14-1099-2014, 2014.
539 Brenot, H., Theys, N., Clarisse, L., van Gent, J., Hurtmans, D. R., Vandenbussche, S., Papagiannopoulos, N., Mona, L.,
540 Virtanen, T., Uppstu, A., Sofiev, M., Bugliaro, L., Vázquez-Navarro, M., Hedelt, P., Parks, M. M., Barsotti, S., Coltelli,
541 M., Moreland, W., Arnold-Arias, D., Hirtl, M., Peltonen, T., Lahtinen, J., Sievers, K., Lipok, F., Rüfenacht, R., Haefele,
542 A., Hervo, M., Wagenaar, S., Som de Cerff, W., de Laat, J., Apituley, A., Stammes, P., Laffineur, Q., Delcloo, A., Lennart,
543 R., Rokitansky, C.-H., Vargas, A., Kerschbaum, M., Resch, C., Zopp, R., Plu, M., Peuch, V.-H., Van Roozendael, M., and
544 Wotawa, G.: EUNADICS early warning system dedicated to support aviation in case of crisis from natural airborne hazard
545 and radionuclide cloud, Nat. Hazards Earth Syst. Sci. Discuss. [preprint], https://doi.org/10.5194/nhess-2021-105,
546 accepted, 2021.
547 Carboni, E., Grainger, R., Walker, J., Dudhia, A., and Siddans, R.: A new scheme for sulphur dioxide retrieval from IASI
548 measurements: application to the Eyjafjallajökull eruption of April and May 2010, Atmos. Chem. Phys., 12, 11417–11434,
549 https://doi.org/10.5194/acp-12-11417-2012, 2012.
550 Carboni, E., R.G. Grainger, T.A. Mather, D.M. Pyle G.E. Thomas, R. Siddans, A.J.A. Smith, A. Dudhia, M.E. Koukouli and
551 D. Balis, The vertical distribution of volcanic SO_2 plumes measured by IASI, Atmospheric Chemistry and Physics, 16,
552 4343– 4367, 2016. (doi:10.5194/acp-16-4343-2016)
553 Carn, S. A., K. Yang, A. J. Prata and N. A. Krotkov, Extending the long-term record of volcanic SO_2 emissions with the Ozone
554 Mapping and Profiler Suite (OMPS) Nadir Mapper, Geophys. Res. Lett., 42, 925-932, doi:10.1002/2014GL062437, 2015.

555 Carn, S. A., L. Clarisse, A.J. Prata, Multi-decadal satellite measurements of global volcanic degassing, Journal of Volcanology
556 and Geothermal Research, 311, 99-134, ISSN 0377-0273, https://doi.org/10.1016/j.jvolgeores.2016.01.002, 2016.
557 Clarisse, L., Coheur, P.-F., Theys, N., Hurtmans, D., and Clerbaux, C.: The 2011 Nabro eruption, a SO_2 layer height analysis
558 using IASI measurements, Atmos. Chem. Phys., 14, 3095-3111, https://doi.org/10.5194/acp-14-3095-2014, 2014.
559 Clarisse, L., Hurtmans, D., Clerbaux, C., Hadji-Lazaro, J., Ngadi, Y., and Coheur, P.-F.: Retrieval of sulphur dioxide from the
560 infrared atmospheric sounding interferometer (IASI), Atmos. Meas. Tech., 5, 581-594, doi:10.5194/amt-5-581-2012, 2012.
561 de Laat, A., Vazquez-Navarro, M., Theys, N., and Stammes, P.: Analysis of properties of the 19 February 2018 volcanic
562 eruption of Mount Sinabung in TROPOMI/S5P and Himawari-8 satellite data, Nat. Hazards Earth Syst. Sci., 20, 1203–
563 1217, https://doi.org/10.5194/nhess-20-1203-2020, 2020.
564 de Leeuw, J., Schmidt, A., Witham, C. S., Theys, N., Taylor, I. A., Grainger, R. G., Pope, R. J., Haywood, J., Osborne, M.,
565 and Kristiansen, N. I.: The 2019 Raikoke volcanic eruption – Part 1: Dispersion model simulations and satellite retrievals
566 of volcanic sulfur dioxide, Atmos. Chem. Phys., 21, 10851–10879, https://doi.org/10.5194/acp-21-10851-2021, 2021.
567 Eckhardt, S., Prata, A. J., Seibert, P., Stebel, K., and Stohl, A.: Estimation of the vertical profile of sulfur dioxide injection into
568 the atmosphere by a volcanic eruption using satellite column measurements and inverse transport modeling, Atmos. Chem.
569 Phys., 8, 3881–3897, https://doi.org/10.5194/acp-8-3881-2008, 2008.
570 European Centre for Medium-Range Weather Forecasts (2012): ECMWF Operational Regular Gridded Data at 1.125 degrees
571 resolution. NCAS British Atmospheric Data Centre, 12th July 2021.
572 https://catalogue.ceda.ac.uk/uuid/a67f1b4d9db7b1528b800ed48198bdac
573 Efremenko, D.S., Loyola, D.G.R., Hedelt, P., and Spurr, R.J.D. Volcanic SO_2 plume height retrieval from UV sensors using a
574 full-physics inverse learning machine algorithm, International Journal of Remote Sensing, 38, sup1, 1-27, doi:
575 10.1080/01431161.2017.1348644, 2017
576 Fedkin, N. M., Li, C., Krotkov, N. A., Hedelt, P., Loyola, D. G., Dickerson, R. R., and Spurr, R.: Volcanic SO_2 effective layer
577 height retrieval for the Ozone Monitoring Instrument (OMI) using a machine-learning approach, Atmos. Meas. Tech., 14,
578 3673–3691, https://doi.org/10.5194/amt-14-3673-2021, 2021.
579 Hedelt, P. and Koukouli, M. E.: S5p+I - SO_2 Layer Height Algorithm Theoretical Baseline Document (ATBD),
580 https://doi.org/10.5281/zenodo.5118540, 2021.
581 Hedelt, P., Efremenko, D. S., Loyola, D. G., Spurr, R., and Clarisse, L.: Sulfur dioxide layer height retrieval from Sentinel-5
582 Precursor/TROPOMI using FP_ILM, Atmos. Meas. Tech., 12, 5503–5517, https://doi.org/10.5194/amt-12-5503-2019,
583 2019.
584 Hughes, E. J., Sparling, L. C., Carn, S. A., and Krueger, A. J.(2012), Using horizontal transport characteristics to infer an
585 emission height time series of volcanic SO_2, *J. Geophys. Res.*, 117, D18307, doi:10.1029/2012JD017957.
586 Hyman, D. M. and Pavolonis, M. J.: Probabilistic retrieval of volcanic SO_2 layer height and partial column density using the
587 Cross-track Infrared Sounder (CrIS), Atmos. Meas. Tech., 13, 5891–5921, https://doi.org/10.5194/amt-13-5891-2020,
588 2020.

589 ICAO: International Civil Aviation Organization, Flight Safety and Volcanic Ash, Doc 9974 AN/487, 999 University Street,
590 Montréal, Quebec, Canada, https://www.icao.int/publications/Documents/9974_en.pdf, last access: 14.10.2021, 2012.
591 Inness, A., Ades, M., Balis, D., Efremenko, D., Flemming, J., Hedelt, P., Koukouli, M.-E., Loyola, D., and Ribas, R.: The
592 CAMS volcanic forecasting system utilizing near-real time data assimilation of TROPOMI/S5P SO2 retrievals, Geosci.
593 Model Dev. Discuss. (preprint), https://doi.org/10.5194/gmd-2021-219, in review, 2021.
594 Jing F, Chauhan A, P Singh R, Dash P. Changes in Atmospheric, Meteorological, and Ocean Parameters Associated with the
595 12 January 2020 Taal Volcanic Eruption. *Remote Sensing*. 2020; 12(6):1026. https://doi.org/10.3390/rs12061026.
596 Kim, M.-H., Omar, A. H., Tackett, J. L., Vaughan, M. A., Winker, D. M., Trepte, C. R., Hu, Y., Liu, Z., Poole, L. R., Pitts, M.
597 C., Kar, J., and Magill, B. E.: The CALIPSO version 4 automated aerosol classification and lidar ratio selection algorithm,
598 Atmos. Meas. Tech., 11, 6107–6135, https://doi.org/10.5194/amt-11-6107-2018, 2018.
599 Kloss, C., Berthet, G., Sellitto, P., Ploeger, F., Taha, G., Tidiga, M., Eremenko, M., Bossolasco, A., Jégou, F., Renard, J.-B.,
600 and Legras, B.: Stratospheric aerosol layer perturbation caused by the 2019 Raikoke and Ulawun eruptions and their
601 radiative forcing, Atmos. Chem. Phys., 21, 535–560, https://doi.org/10.5194/acp-21-535-2021, 2021.
602 Koffi, B., Schulz, M., Bréon, F.-M., Griesfeller, J., Winker, D., Balkanski, Y., Bauer, S., Berntsen, T., Chin, M., Collins, W.
603 D., Dentener, F., Diehl, T., Easter, R., Ghan, S., Ginoux, P., Gong, S., Horowitz, L. W., Iversen, T., Kirkevåg, A., Koch,
604 D., Krol, M., Myhre, G., Stier, P., and Takemura, T.: Application of the CALIOP layer product to evaluate the vertical
605 distribution of aerosols estimated by global models: AeroCom phase I results, J. Geophys. Res.-Atmos., 117, D10,
606 https://doi.org/10.1029/2011JD016858, 2012.
607 Koukouli, M. E., Balis, D., Michailidis, K, Hedelt, P.: S5p+I - SO_2 Layer Height Validation Report (VR),
608 https://doi.org/10.5281/zenodo.5118558, 2021.
609 Koukouli, M.E, D. Balis, S. Dimopoulos, & N. Siomos, SACS-2/SMASH – Validation Report on the Eyjafjallajökull and
610 Grimsvötn eruptions (v1.0). Zenodo. https://doi.org/10.5281/zenodo.5566654, 2014.
611 Lopes, F. J. S., Silva, J.J., Antuña Marrero, J.C., Taha, G. and Landulfo, E., Synergetic Aerosol Layer Observation after the
612 2015 Calbuco Volcanic Eruption Event. *Remote Sens.*, *11*, 195. https://doi.org/10.3390/rs11020195, 2019.
613 Loyola, D. G., Pedergnana, M., and Gimeno Garcia, S., Smart sampling and incremental function learning for very large high
614 dimensional data. Neural Networks, https://doi.org/10.1016/j.neunet.2015.09.001, 78:75–87, 2016.
615 Loyola, D. G., Xu, J., Heue, K.-P., and Zimmer, W.: Applying FP_ILM to the retrieval of geometry-dependent effective
616 Lambertian equivalent reflectivity (GE_LER) daily maps from UVN satellite measurements, Atmos. Meas. Tech., 13, 985–
617 999, https://doi.org/10.5194/amt-13-985-2020, 2020.
618 McKee, Kathleen, Cassandra M. Smith, Kevin Reath, Eveanjelene Snee, Sean Maher, Robin S. Matoza, Simon Carn, Larry
619 Mastin, Kyle Anderson, David Damby, Diana C. Roman, Artem Degterev, Alexander Rybin, Marina Chibisova, Jelle D.
620 Assink, Rodrigo de Negri Leiva, Anna Perttu, Evaluating the state-of-the-art in remote volcanic eruption characterization
621 Part I: Raikoke volcano, Kuril Islands, Journal of Volcanology and Geothermal Research, Volume 419, 107354, ISSN
622 0377-0273, https://doi.org/10.1016/j.jvolgeores.2021.107354, 2021.

Nanda, S., de Graaf, M., Veefkind, J. P., Sneep, M., ter Linden, M., Sun, J., and Levelt, P. F.: A first comparison of TROPOMI aerosol layer height (ALH) to CALIOP data, Atmos. Meas. Tech., 13, 3043–3059, https://doi.org/10.5194/amt-13-3043-2020, 2020.

Omar, A., Winker, D., Kittaka, C., Vaughan, M., Liu, Z., Hu, Y. X., Trepte, C., Rogers, R., Ferrare, R., Lee, K., Kuehn, R., and Hostetler, C.: The CALIPSO automated aerosol classification and lidar ratio selection algorithm, J. Atmos. Ocean. Tech., 26,1994–2014, doi:10.1175/2009jtecha1231.1, 2009.

Pardini, Federica, Mike Burton, Fabio Arzilli, Giuseppe La Spina, Margherita Polacci, SO_2 emissions, plume heights and magmatic processes inferred from satellite data: The 2015 Calbuco eruptions, Journal of Volcanology and Geothermal Research, Volume 361, 2018, Pages 12-24, ISSN 0377-0273, https://doi.org/10.1016/j.jvolgeores.2018.08.001, 2018.

Perttu, Anna, Benoit Taisne, Silvio De Angelis, Jelle D. Assink, Dorianne Tailpied, Ross Adrian Williams, Estimates of plume height from infrasound for regional volcano monitoring, Journal of Volcanology and Geothermal Research, 402, 106997, ISSN 0377-0273, https://doi.org/10.1016/j.jvolgeores.2020.106997, 2020.

Prata, A. T., Young, S. A., Siems, S. T., and Manton, M. J.: Lidar ratios of stratospheric volcanic ash and sulfate aerosols retrieved from CALIOP measurements, Atmos. Chem. Phys., 17, 8599–8618, https://doi.org/10.5194/acp-17-8599-2017, 2017.

Prata, A.J. Satellite detection of hazardous volcanic clouds and the risk to global air traffic. *Nat Hazards* **51,** 303–324 (2009). https://doi.org/10.1007/s11069-008-9273-z

Reichardt U, Ulfarsson GF, Petursdottir G. Cooperation Between Science and Aviation-Sector Service Providers in Europe for Risk Management of Volcanic Ash. Transportation Research Record. 2017;2626(1):99-105. doi:10.3141/2626-12

Saunders, R. W., Matricardi, M., and Brunel, P.: An improved fast radiative transfer model for assimilation of satellite radiance observations, Q. J. Roy. Meteor. Soc., 125, 1407-1425,https://doi.org/10.1002/qj.1999.49712555615, 1999

Tournigand, P-Y, Valeria Cigala, Alfredo J. Prata, Andrea K. Steiner, Gottfried Kirchengast, Hugues Brenot, Lieven Clarisse and Riccardo Biondi, The 2015 Calbuco Volcanic Cloud Detection Using GNSS Radio Occultation and Satellite Lidar, IGARSS 2020 - 2020 IEEE International Geoscience and Remote Sensing Symposium, 2020, pp. 6834-6837, doi: 10.1109/IGARSS39084.2020.9323356

Vaughan, M., Pitts, M., Trepte, C., Winker, D., Detweiler, P., Garnier, A., Getzewich, B., Hunt, W., Lambeth, J., Lee, K.-P., Lucker, P., Murray, T., Rodier, S., Tremas, T., Bazureau, A., and Pelon, J.: Cloud-Aerosol LIDAR Infrared Pathfinder Satellite Observations (CALIPSO) data management system data products catalog, Release 4.92, NASA Langley Research Center Document PC-SCI-503, available at: https://www-calipso.larc.nasa.gov/products/CALIPSO_DPC_Rev4x92.pdf, last access: 14 September 2020, 225 pp., 2020.

Vira, J., E. Carboni, R. G. Grainger and M. Sofiev, Variational assimilation of IASI SO_2 layer height and total column retrievals in the 2010 eruption of Eyjafjallajökull using the SILAM v5.3 chemistry transport model, Geosci. Model Dev., 10, 1985-2008, doi:10.5194/gmd-10-1985-2017, 2017.

656 Walker, J. C., Dudhia, A., and Carboni, E.: An effective method for the detection of trace species demonstrated using the
657 MetOp Infrared Atmospheric Sounding Interferometer, Atmos. Meas. Tech., 4, 1567–1580, https://doi.org/10.5194/amt-4-
658 1567-2011, 2011.
659 Walker, J.C., E. Carboni, A. Dudhia and R.G. Grainger, Improved detection of sulphur dioxide in volcanic plumes using
660 satellite-based hyperspectral infrared measurements: Application to the Eyjafjallajökull 2010 eruption, Journal of
661 Geophysical Research, 117, D00U16, https://doi.org/10.1029/2011JD016810, 2012.
662 Wang, J., S. Park, J. Zeng, K. Yang, S. Carn, N. Krotkov, and A. H. Omar, Modeling of 2008 Kasatochi volcanic sulphate
663 direct radiative forcing: assimilation of OMI SO_2 layer height data and comparison with MODIS and CALIOP
664 observations, Atmos. Chem. Phys., 13, 1895-1912, doi:10.5194/acp-13-1895-2013, 2012.
665 Winker, D. M., Z. Liu, A. Omar, J. Tackett, and D. Fairlie, CALIOP observations of the transport of ash from the
666 Eyjafjallajökull volcano in April 2010, J. Geophys. Res., 117, D00U15, doi:10.1029/2011JD016499, 2012.
667 Winker, D., Pelon, J., Coakley, J., Ackerman, S., Charlson, R., Colarco, P., Flamant, P., Fu, Q., Hoff, R., Kittaka, C., Kubar,
668 T., Le Treut, H., McCormick, M., Megie, G., Poole, L., Powell, K., Trepte, C., Vaughan, M., and Wielicki, B.: The
669 CALIPSO Mission: a global 3-D view of aerosols and clouds, B. Am. Meteorol. Soc., 91, 1211–1229,
670 https://doi.org/10.1175/2010BAMS3009.1, 2010.
671 Xu, J., Schüssler, O., Loyola Rodriguez, D. G., Romahn, F., and Doicu, A.: A novel ozone profile shape retrieval using Full-
672 Physics Inverse Learning Machine (FP_ILM), IEEE J. Sel. Topics Appl. Earth Observ. Remote Sens., 10, 5442–5457,
673 https://doi.org/10.1109/JSTARS.2017.2740168, 2017.
674 Zehner, C., Ed. (2012). Monitoring Volcanic Ash from Space. ESA–EUMETSAT workshop on the 14 April to 23 May 2010
675 eruption at the Eyjafjöll volcano, South Iceland (ESA/ESRIN, 26–27 May 2010) ESA Publication STM-280.
676 doi:10.5270/atmch-10-01.